frontiers | Frontiers in Marine Science

TYPE Original Research
PUBLISHED 13 December 2023
DOI 10.3389/fmars.2023.1329338

Check for updates

OPEN ACCESS

EDITED BY
Xingsen Guo,
University College London,
United Kingdom

REVIEWED BY
Chuanyuan Wang,
Chinese Academy of Sciences (CAS), China
Youwei Wang,
University of Virginia, United States

*CORRESPONDENCE
Entao Liu
liuentao@cug.edu.cn

RECEIVED 28 October 2023
ACCEPTED 27 November 2023
PUBLISHED 13 December 2023

CITATION
Liu E, Luo W, Yan D, Deng Y, Chen S, Zhong J and Jiao Y (2023) Depositional evolution in response to long-term marine transgression in the northern South China Sea.
*Front. Mar. Sci.* 10:1329338.
doi: 10.3389/fmars.2023.1329338

COPYRIGHT
© 2023 Liu, Luo, Yan, Deng, Chen, Zhong and Jiao. This is an open-access article distributed under the terms of the Creative Commons Attribution License (CC BY). The use, distribution or reproduction in other forums is permitted, provided the original author(s) and the copyright owner(s) are credited and that the original publication in this journal is cited, in accordance with accepted academic practice. No use, distribution or reproduction is permitted which does not comply with these terms.

# Depositional evolution in response to long-term marine transgression in the northern South China Sea

Entao Liu[1,2]*, Wei Luo[3], Detian Yan[4], Yong Deng[5], Si Chen[4], Jialin Zhong[1] and Yangshuo Jiao[1]

[1]Hubei Key Laboratory of Marine Geological Resources, China University of Geosciences, Wuhan, China, [2]Radiogenic Isotope Facility, School of Earth and Environmental Sciences, The University of Queensland, Brisbane, QLD, Australia, [3]Hainan Branch Company, China National Offshore Oil Corporation, Haikou, China, [4]Key Laboratory of Tectonics and Petroleum Resources, Ministry of Education, China University of Geosciences, Wuhan, China, [5]Zhanjiang Branch Company, China National Offshore Oil Corporation, Zhanjiang, China

Research on the interaction between depositional evolution process and marine transgression is critical to understanding the transform mechanism of sedimentary systems and guiding hydrocarbon exploration. The early Miocene witnessed the most significant sea-level rise since the Cenomanian, which resulted in extensive marine-influenced deposits worldwide. However, the relationship between the process of depositional evolution and long-term marine transgressions (>1 Ma) remains poorly understood. The Pearl River Mouth Basin in the South China Sea offers a comprehensive deposition record of the early Miocene marine transgression. This study employs high-quality 3D seismic, well-logging, and core data to investigate the impact of the early Miocene transgression on the evolutionary dynamics of the sedimentary system. The regional sea level exhibited a prolonged rise of at least 100 m during the deposition period of the Miocene Zhujiang Formation, corresponding to the long-term marine transgressive in the South China Sea. Throughout this marine transgression, depositional systems developed in the study area include tidal flats, fan deltas, meandering river deltas, and shallow marine shelf sand bodies. The marine transgression process resulted in a significant change in depositional system types, which can be divided into seven units from Unit 1 at the bottom to Unit 7 at the top. The predominant deposition environment transitioned from tidal flats in Units 1-3 to meandering river deltas in Units 4-5, and finally to shallow marine shelf systems in Units 6-7. In the early stage (Units 1-3), the regional uplifts hindered sea level transgression and caused erosion, leading to the development of small-scale proximal fan deltas. In the middle stage (Units 4-5), these regional uplifts submerged, and meandering river deltas dominated with sediments derived from distant extrabasinal sources. During the late stage (Units 6-7), regional sea levels reached their peak, transforming the entire basin into a shallow marine shelf system. Additionally, this marine transgression significantly influenced the distribution of hydrocarbon resources. Notably, the shallow marine shelf sand bodies in Units 6-7 warrant

substantial attention for future exploration. This study outlines the complicated transitional processes within depositional systems during long-term marine transgression events, holding relevance for the global evolution of marginal sea basins.

KEYWORDS

depositional system, depositional evolution, hydrocarbon resources, South China Sea, marginal sea

# 1 Introduction

Sedimentary strata in marginal sea basins play a crucial role in recording important geological signals during deposition (Andrés et al., 2011; Wang et al., 2014; Bogemans et al., 2016; Shao et al., 2016). These signals include processes such as weather denudation, sediment transport, and deep-ocean deposition. Understanding the relationship between the depositional evolution processes and sea level changes is key to uncovering sedimentary processes, identifying controlling mechanisms of depositional systems, and predicting potential reservoirs (Choi et al., 2008; Liu et al., 2009; Rossetti et al., 2013; Li et al., 2019). While this connection has been extensively studied in Quaternary marine deposits (e.g., Andrés et al., 2011; Wang et al., 2014; Zhou et al., 2014; Tang et al., 2018; Guo et al., 2023a; Guo et al., 2023b), research on pre-quaternary strata is relatively limited (e.g., Rossetti et al., 2013; Poisson et al., 2016).

The early Miocene period (23.3 Ma-16.3 Ma) holds significant importance in Earth's geological timescale as it witnessed the most substantial sea-level rise since the Oligo-Miocene transition (Müller et al., 2008; Rossetti et al., 2013). Although the magnitude of this rise is still a topic of debate, with estimates ranging from 180 m to tens of meters above the current sea level (Haq et al., 1987; Miller et al., 2005), it is undisputed that a long time-scale marine transgression occurred in the early Miocene (Rossetti et al., 2013; Fu et al., 2019). Evidently, major marine transgression events have been observed worldwide, especially in numerous continental margins (Poisson et al., 2016). Therefore, studying the early Miocene strata in marginal sea basins presents an ideal opportunity to investigate the response of depositional evolution to long-term marine transgression. However, compared to the extensively studied Quaternary strata, there have been fewer attempts to study the early Miocene deposits (Rossetti et al., 2013; Poisson et al., 2016), primarily because of the limited availability of continuous drilling and lithology data related to the Miocene marine transgression event. More importantly, such an attempt is critical for understanding the long-term (> 1 Ma) depositional evolution process during a long-term marine transgression.

The South China Sea, located along the western Pacific margin, is recognized as the largest marginal sea basin and has attracted considerable attention from geologists due to its unique structural characteristics and abundant hydrocarbon resources (Shao et al., 2016; Liu et al., 2022a; Wang et al., 2022). The Pearl River Mouth Basin (PRMB), situated on the northern margin of the South China Sea continental shelf, is particularly noteworthy as a hydrocarbon-bearing basin (Huang et al., 2003; Quan et al., 2015). Recent drilling findings have revealed the remarkable potential of Eocene-Miocene strata in the PRMB, making it a focal point for hydrocarbon exploration (Xie et al., 2021; Fu et al., 2022). Previous studies (e.g., Xie et al., 2014; Liu et al., 2022a; Liu et al., 2022b; Wang et al., 2022) have extensively documented the complex structural evolution of the PRMB, spanning from the Eocene lacustrine environment to the Miocene marine environment. Within the basin, various depositional systems, including fan deltas, tidal flats, and lacustrine deposits, have been identified (Xie et al., 2014; Liu et al., 2022b). Notably, during this evolution, the early Miocene Zhujiang Formation experienced a significant long-term marine transgression, evident from the widespread development of onlaps in seismic profiles surrounding uplifted areas (Xie et al., 2014; Liu et al., 2022b). Consequently, this period witnessed a rapid evolution of depositional systems (Liu et al., 2022b). Therefore, the PRMB offers a highly valuable target for gaining deeper insights into the depositional evolution process during the global Miocene transgressive event.

It is crucial to understand how depositional systems evolve in the background of long-term marine transgression and their impact on the distribution of depositional facies during marine transgression. Although previous studies (e.g., Xie et al., 2014; Zeng et al., 2019; Quan et al., 2020; Liu et al., 2022b) have extensively investigated the depositional systems in the PRMB, the focus has mainly been on the Eocene and Oligocene strata. There is limited research on the Miocene Zhujiang Formation (Wang et al., 2021), and studies on its long-term evolutionary characteristics are scarce. Furthermore, the Miocene Zhujiang Formation has recently gained importance in hydrocarbon exploration, but the presence of oil and gas reservoirs in different types of depositional systems remains unclear (Xie et al., 2021; Fu et al., 2022). Hence, studying the depositional evolution process in the Miocene Zhujiang Formation can not only enhance the understanding of depositional evolution in response to marine transgressions but also provide valuable evidence for hydrocarbon exploration and development within the Miocene Zhujiang Formation.

To gain a better understanding of the internal stratigraphic architecture and depositional evolution process, a high-precision sequence framework scheme is essential (Shanley and McCabe, 1994; Zecchin and Catuneanu, 2015; Liu et al., 2022b). This study aims to investigate the early Miocene Zhuajiang Formation in the PRMB using

newly acquired 3D seismic data and over 40 wells, alongside sequence stratigraphy theory. The main objectives are: (1) characterizing the depositional systems and their distribution in the early Miocene Zhuajiang Formation; (2) uncovering the long-term depositional evolution process during the early Miocene; (3) providing a new case study to comprehend the relationship between depositional evolution and long-term marine transgression.

## 2 Geological setting

The South China Sea is situated at the convergence point of the Eurasian, Pacific, and Indian Ocean tectonic plates, bordered by South China-Indochina blocks to the northwest and Borneo-Philippines blocks to the southeast (Figure 1). This region has undergone intricate structural and depositional transformations, encompassing multiple sedimentary basins (Hayes and Nissen, 2005; Franke, 2013). PRMB is a significant offshore petroleum-rich basin located in the central part of the northern South China Sea margin, covering an area of approximately $27\times10^4$ km$^2$ (Figure 1). It consists of four sedimentary depressions: Zhu I Depression, Zhu II Depression, Zhu III Depression, and Chaoshan Depression (Figure 1), with its basement consisting of Paleozoic quartzite and metamorphic rocks. Acting as a Cenozoic continental margin extension basin, the PRMB has undergone three major tectonic phases: a syn-rift stage (49-30 Ma) during the Eocene, a transition stage (30-16.3 Ma) from the Oligocene to the early Miocene, and a post-rift stage (16.3 Ma to the present) from the middle Miocene to the Quaternary (Hayes and Nissen, 2005; Zhu et al., 2010; Xie et al., 2014; Clift et al., 2015) (Figure 2). These phases are associated with four Cenozoic tectonic events (i.e., the first and second episodes of the Zhuqiong Event, Nanhai Event, and Baiyun Event), marked by four regional unconformities (T90, T80, T70, T60) (Figure 2).

Focusing on the target study area, the Zhu III Depression, located offshore in the western PRMB, spans 12,000 km$^2$ and reaches water depths of 0 to 360 m (Figure 1). The syn-rift stage (49-30 Ma) can be divided into two phases: the deposition of the Wenchang Formation (49-39 Ma) and the formation of the Enping Formation (39-30 Ma) (Figure 2). These formations are characterized by deltaic-lacustrine deposits, such as fan deltas, braided river deltas, and beach bars, which serve as the main source rocks for hydrocarbons in the PRMB (Shao et al., 2016; Zeng et al., 2019; Quan et al., 2020; Liu et al., 2022b). The sediments were mainly eroded from nearby Shenhu Uplift, Qionghai Uplift, and Hainan Island (Liu et al., 2022a). The transition stage (30-16.3 Ma) is marked by the Zhujiang and Zhuhai Formations, which act as the primary reservoirs in the depression. The Zhuhai Formation (30-23.3 Ma) primarily features semi-enclosed bays, tidal flats, and deltas, while the early Miocene Zhujiang Formation (23.3-16.3 Ma) demonstrates the rapid evolution of depositional systems, including fan deltas, tidal flats, meandering river deltas, and shallow marine shelf sand bodies (Zhou et al., 2015; Shao et al., 2016; Wang et al., 2021; Liu et al., 2022b) (Figure 2). The sediments for meandering river deltas and shallow marine shelf sand bodies were provided by the Pearl River system (Liu et al., 2022a). During the deposition of the Zhujiang Formation, a substantial marine transgression occurred, leading to the influx of marine sediments (Haq et al., 1987; Mao et al., 2019; Ge et al., 2022; Liu et al., 2022a) (Figure 2). Sequence stratigraphy analysis divides the Zhujiang Formation into

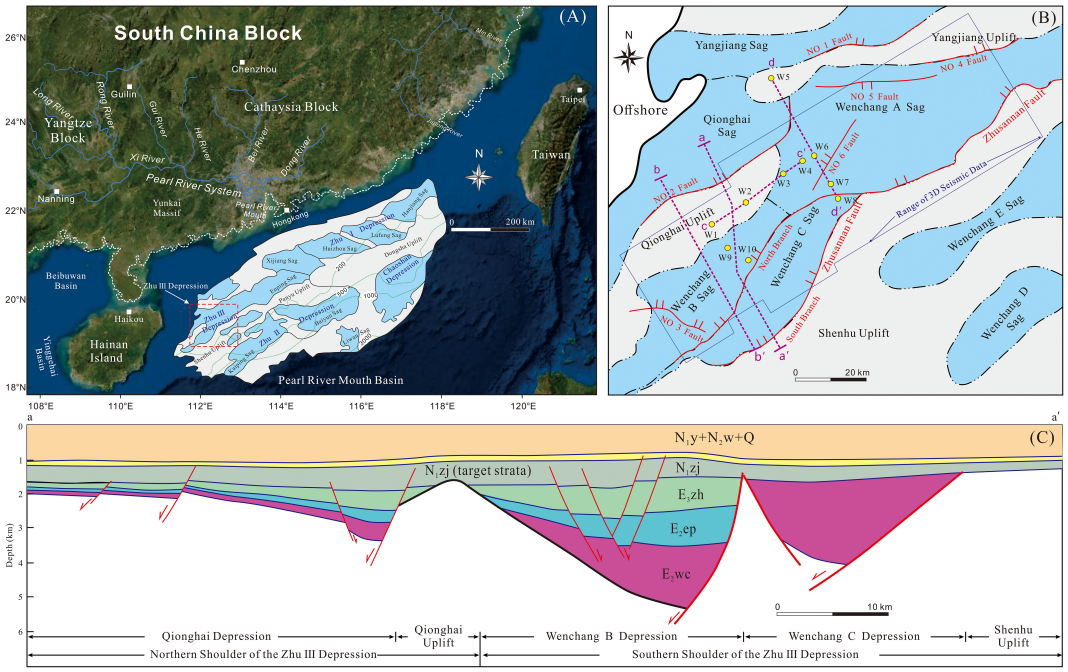


FIGURE 1
**(A)** Geological map showing the regional setting of the PRMB (modified after Liu et al., 2022a). **(B)** Map showing tectonic elements of the Zhu III Depression and locations of seismic profiles. **(C)** Interpreted NE-trending profile in the Zhu III Depression and the location of the profile is shown in **(B)**.

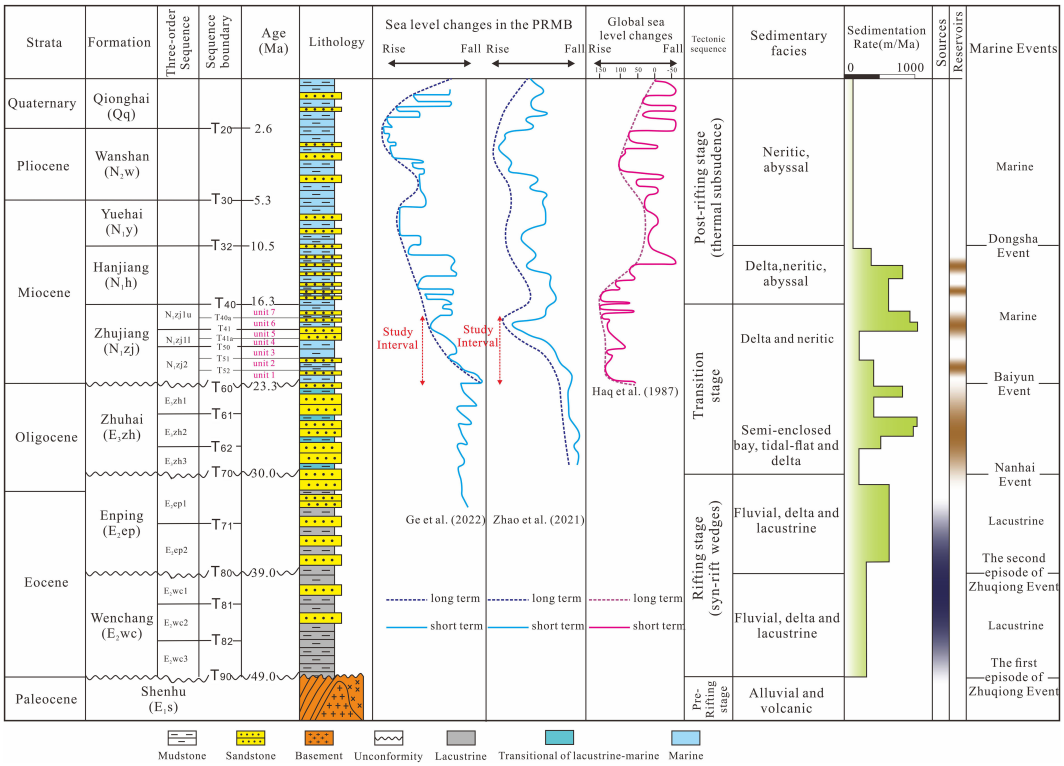


FIGURE 2
Generalized stratigraphic framework, sedimentary facies, tectonic evolution, and source-reservoir-cap assemblages of the PRMB (modified after Xie et al., 2014 and Wang et al., 2018. The sediment rate curve is from Xie et al., 2014, and the sea level curves are from Haq et al., 1987. Zhao et al., 2001, and Ge et al., 2022.

seven sedimentation units (Units 1 to 7) (Liu et al., 2022b). The lower and middle intervals (Units 1-5) are characterized by sandstone interbedded with limestone, while the upper interval (Units 6-7) consists mainly of sandstone interbedded with limestone (Zhou et al., 2015; Liu et al., 2022b) (Figure 2). Subsequent Miocene Hanjiang and Miocene Yuehai Formations, as well as Pliocene Wanshan Formations and Quaternary deposits, were all laid down in a marine depositional environment, dominated by siliciclastic interbedded fine-grained sandstones and mudstones (Zhou et al., 2015) (Figure 2).

# 3 Methods

The research methodology employed a combination of seismic data, drilling cores, logging data, and lithology data provided by China National Offshore Oil Corporation (CNOOC). These data sets were used to conduct sedimentological and sequence stratigraphic studies. The seismic data covered an area of approximately 2000 km$^2$, with a peak frequency of around 40 Hz. The 3D seismic survey comprises regular spacing intervals, with a distance of 12.5 m along the inline direction and 25 m along the crossline direction. Calibrating the seismic data with well data was done using synthetic seismogram calibration. The sequence stratigraphic technique (Shanley and McCabe, 1994; Zecchin and Catuneanu, 2015) was applied to establish a framework across the depression and identify different stratal stacking patterns in various structural units. In total, eight sequence boundaries were identified using well-log and seismic data and were interpreted accordingly, dividing the Zhujiang Formation into seven depositional units, which are labeled Units 1-7 (Figure 2). Eight sequence boundaries (T60, T52, T51, T50, T41a, T41, T40a, T40 from base to top) were identified and regionally tracked (Figures 3, 4).

The identification and categorization of depositional systems or elements mainly depends on the lithofacies associations and internal architectures or geometries of the depositional systems (Wang et al., 2021). Geological and geophysical methods were utilized to determine the types and ranges of depositional systems. Sedimentary facies and depositional characteristics were described using over 400 m of drilling cores obtained from 15 wells. As drilling cores were limited in the study area, logging and lithological association data from over 40 wells were also employed. This data includes natural gamma, true resistivity, and acoustic logging data, which help identify depositional facies and constrain their distribution ranges. In areas without drilling cores, the ranges of depositional systems were determined using 3D seismic data. Techniques such as seismic reflection, horizontal slice, and attributive analysis were performed on the Geoframe® software to extract this data. A comprehensive interpretation of depositional systems and facies architecture is conducted by analyzing the lithofacies associations and architectures, as well as the geometries observed in well logs, seismic sections, and RMS

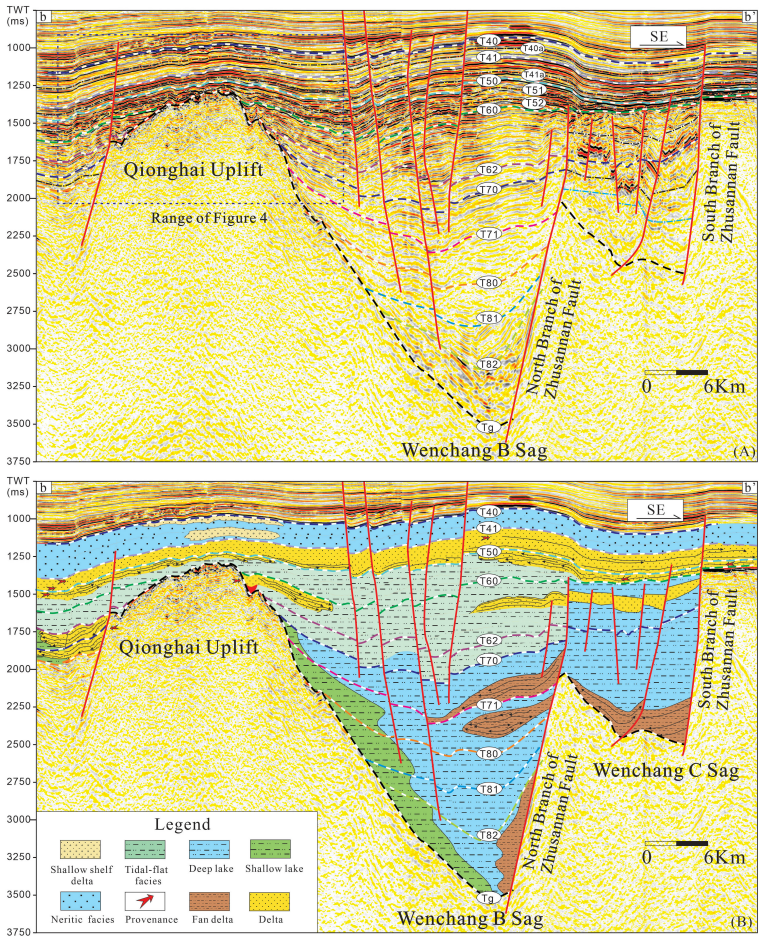


FIGURE 3
**(A)** interpreted seismic section bb' showing seismic reflection characteristics and the depositional evolution in the PRMB; **(B)** the types of depositional facies and their distribution ranges in the section bb' showing the depositional evolution from the Eocene to the Miocene. The location of section bb' is shown in Figure 1.

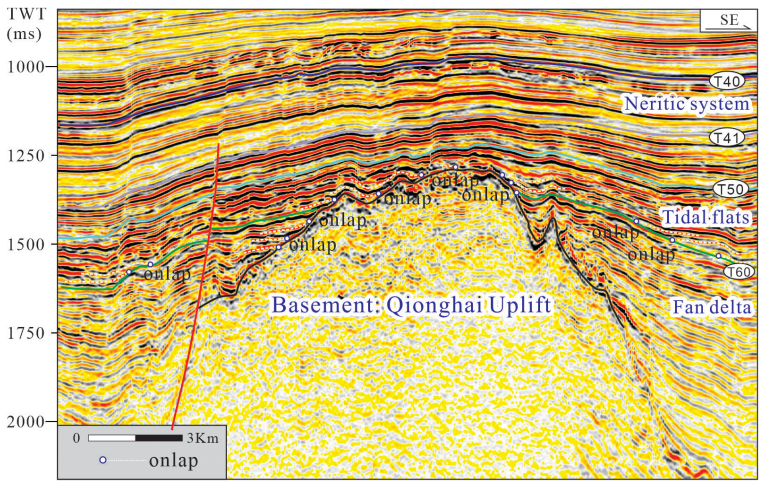


FIGURE 4
Interpreted seismic profile showing seismic reflection characteristics and the depositional evolution in the Zhujiang Formation. The range of this region is shown in Figure 3.

amplitude slices. The Palaeogeographic maps of Horizon T40 and T60 were generated using the Petrel® software.

# 4 Results

## 4.1 Lithofacies associations and depositional facies

Through a comprehensive analysis of core samples, well logs, and seismic sections, we have identified 13 types of lithofacies associations (FA1-FA13) within the Zhujiang Formation in the PRMB and outlined in Table 1. These lithofacies associations were interpreted as the deposits of six major depositional facies, including fan delta plain deposits (FA1-FA2), fan delta front deposits (FA3-FA4), meandering river delta front deposits (FA5-FA7), tidal flat deposits (FA8-FA10), shallow marine shelf sand deposits (FA11-FA12) and coastal-shallow marine shelf deposits (FA13) (Table 1).

### 4.1.1 Lithofacies associations FA1-FA2: fan delta plain deposits

#### 4.1.1.1 Description

FA1 comprises conglomeratic sandstones and coarse sandstones exhibiting fining upward patterns and infilling channelized erosion surfaces (Figure 5). It displays box-shaped forms and relatively high gamma values on the gamma logging curves (Figures 6, 7). FA2 is predominantly made up of sandy mudstones and siltstones with abundant bioturbation and deformation structures, characterized by a serrate gamma well-log pattern (Figures 6, 7).

#### 4.1.1.2 Interpretation

FA1 is interpreted as distributary channels, with the fining-upward sandstone bodies representing channel deposits in the proximal reaches of the deltaic plain (Coleman and Wright, 1975; Galloway, 1975). FA2 is interpreted as interdistributary bay deposits (Coleman and Wright, 1975).

TABLE 1 Lithofacies associations and their characteristics in the Miocene Zhujiang Formation in the PRMB.

| Lithofacies Association Code | Description | Interpretation | Depositional Environment |
|---|---|---|---|
| FA1 | Thick beds of conglomeratic sandstones and coarse sandstones, fining upward patterns, infilling channelized erosion surfaces, poorly sorted, box-shaped gamma curves, wedge-shaped seismic reflections, variable amplitude | Distributary channel | Fan delta plain |
| FA2 | Thin layers of sandy mudstones and siltstones, abundant bioturbation and deformation structures, horizontal bedding and wavy bedding, serrate-shaped gamma curves | Interdistributary bay | Fan delta plain |
| FA3 | Thick-bedded fine to coarse-grained sandstones, poorly sorted and subangular, low-angle cross-bedding, deformed mudstone shivers, fining upward patterns, erosion surfaces and gravels, box-shaped gamma curves | Subaqueous distributary channel | Fan delta front |
| FA4 | Thick-bedded siltstones and fine to medium sandstones, small-scale horizontal or wavy cross-bedding, coarsening upward patterns | Estuary bar | Fan delta front |
| FA5 | Thick-bedded fine to medium-grained sandstones, bell- or box-shaped gamma curves, parallel bedding, low-angle cross-bedding, general upward fining patterns | Subaqueous distributary channel | Meandering river delta front |
| FA6 | Medium to thick-bedded fine-grained sandstones and siltstones, general upward coarsening patterns, parallel bedding, funnel-shaped log curves | Estuary bar | Meandering river delta front |
| FA7 | Thin-bedded silty mudstones and siltstones interbedded with thin layers of mudstones, medium funnel shape on the gamma curves, ripple laminae, soft deformation structure and horizontal bedding | Distal bar | Meandering river delta front |
| FA8 | Gray fine-grained sandstones interbedded with cm-mm scale layers of dark gray mudstones to siltstones | Sandy flat | Tidal flat |
| FA9 | interbedded thin layers of sandstones and mudstones, tidal rhythmic bedding, ripple bedding, lenticular bedding and bioturbation structures | Mixed flat | Tidal flat |
| FA10 | Thick layers of mudstones interbedded with thin layers of sandstones, horizontal lamination and widespread strong bioturbation structures | Mud flat | Tidal flat |
| FA11 | Gray fine sandstones, fishbone-shaped cross-bedding and wavy bedding, bimodal box or bell-shaped patterns, low-frequency strong amplitude lens-shaped reflections in the seismic section. | Tidal sand ridge | Shallow shelf sand bodies |
| FA12 | Grayish-white muddy sandstones interbedded with mudstones, upward coarsening patterns, funnel-shaped with high natural gamma values on the natural gamma ray curves, medium frequency, medium amplitude sheet-like reflections in the seismic profile | Offshore bar | Shallow shelf sand bodies |
| FA13 | Thick-bedded gray to black mudstones with interbedded thin layers of siltstones and horizontal bedding | Coastal-shallow shelf deposits | Coastal-shallow shelf deposits |

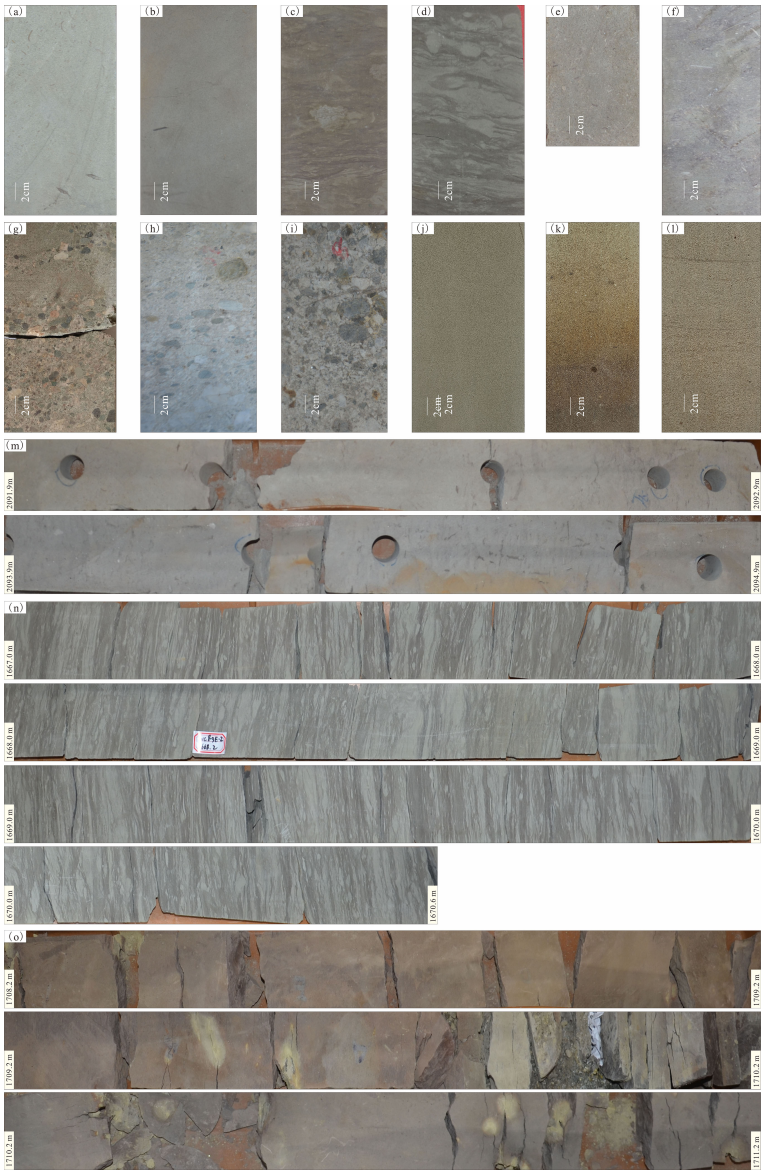

FIGURE 5
Typical sedimentary characteristics of the deposits in the early Miocene Zhujiang Formation. **(A)** 2092.8 m in Well W4, siltstone in Unit 6, interpreted as a shallow marine shelf sand body; **(B)** 2090.2 m in Well W4, fine-grained sandstone in Unit 6, interpreted as a shallow marine shelf sand body; **(C)** 1672.0 m in Well W4, siltstone interbedded with mudstone in Unit 3 interpreted as a sand flat; **(D)** 1668.2 m in Well W4, siltstone interbedded with mudstone in Unit 3 interpreted as a sand flat; **(E)** 2252.3 m in Well W5, fine-grained sandstone with normally graded bedding in Unit 1 interpreted as a underwater distributary channel; **(F)** 2253.2 m in Well W3, fine-grained sandstone with normally graded bedding in Unit 1, interpreted as a underwater distributary channel. **(G-I)** conglomeratic sandstones with normally graded bedding in Unit 2, interpreted as distributary channels; **(J)** 2251.3 m in Well W5, a siltstone in Unit 5 interpreted as a distal bar; **(K, L)** fine-grained sandstones with normally graded bedding interpreted as underwater distributary channels; **(M)** 2.0 m (2091.9-2092.9 m and 2093.9-2094.9 m, Unit 6) long core of the shallow-marine detrital deposits from Well 4, interpreted as shallow marine shelf sand bodies; **(N)** 3.6 m (1667.0-1670.6 m, Unit 3) long core of the tidal flat deposits from W9, interpreted as sand flat deposits; **(O)** 3.0 m (1708.2-1711.2 m, Unit 1) long core of the fan delta front deposits.

#### 4.1.1.3 Distribution

Fan delta deposits were deposited in Units 1-3, with their sediments mainly sourced from the Shenhu and Qionghai Uplifts (Figure 8). They are primarily located on the downthrown block adjacent to the Zhusannan Fault in the northern region and around the Qionghai Uplift (Figure 8). In seismic profiles, fan delta deposits are characterized by wedge-shaped seismic reflections, variable amplitude, and low to medium frequency (Figures 3, 4). These fan delta deposits can be subdivided into two distinct parts: fan delta plain and front deposits (Figure 8). Fan delta plain systems mainly comprise distributary channels and interdistributary bay deposits (Figure 8).

### 4.1.2 Lithofacies associations FA3-FA4: fan delta front deposits

#### 4.1.2.1 Description

FA3 consists of medium to thick-bedded fine to coarse-grained sandstones with poorly sorted and subangular grains (Figures 5, 6,

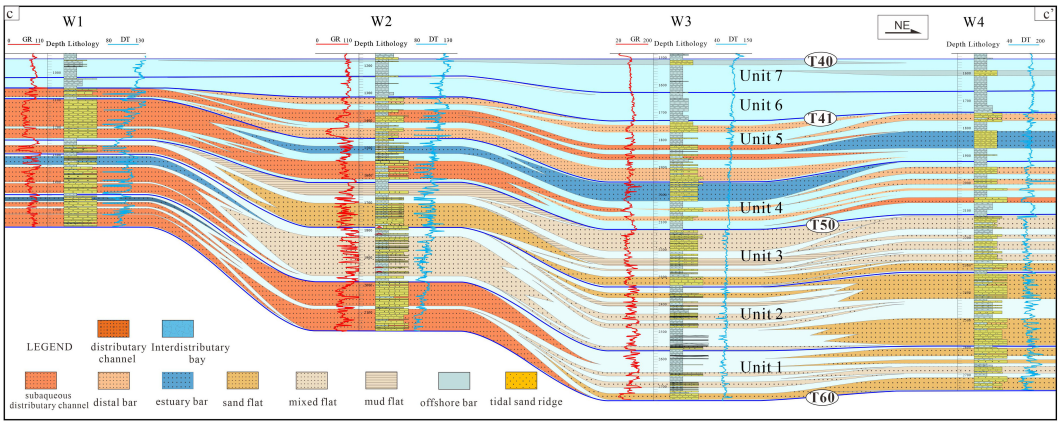


FIGURE 6
Typical sedimentary characteristics showing the sedimentary architecture and depositional evolution process of the Miocene Zhujiang Formation. The well locations are shown in Figure 1B.

7). Low-angle cross-bedding, deformed mudstone shivers, and fining upward patterns are common in this lithofacies association. Erosion surfaces and gravels are also present at the bottom of FA3 (Figure 5). FA4 is composed of thick-bedded siltstones and fine to medium sandstones, exhibiting general upward coarsening patterns, with small-scale horizontal or wavy cross-bedding observed (Figures 5–7).

#### 4.1.2.2 Interpretation

The lithofacies associations of FA3-FA4 are interpreted as fan delta front deposits (Zhang, 2019). FA3 is interpreted as subaqueous distributary channel deposits, as evidenced by the presence of erosion surfaces and fining upward patterns (Coleman and Wright, 1975; Galloway, 1975; Liu et al., 2014). FA4 is interpreted as an estuary bar deposit (Galloway, 1975; Orton and Reading, 1993).

#### 4.1.2.3 Distribution

Similar to the fan delta plain, fan delta front deposits were deposited in Units 1-3 and were located in the downthrown block adjacent to the Zhusannan Fault and the periphery of the Qionghai uplift, but closer to the basin center (Figure 8).

### 4.1.3 Lithofacies associations FA5-FA7: meandering river delta front deposits

#### 4.1.3.1 Description

This lithofacies associations group consists of FA5, FA6, and FA7. Unlike FA3-4, the grains in these lithofacies associations are well-sorted and well-rounded (Figure 5). FA5 is mainly composed of thick bedded, fine to medium-grained sandstones with bell- or box-shaped gamma curves (Figures 6, 7). It exhibits parallel bedding, low-angle cross bedding, and general upward fining patterns (Figure 5). FA6 is primarily made up of medium to thick

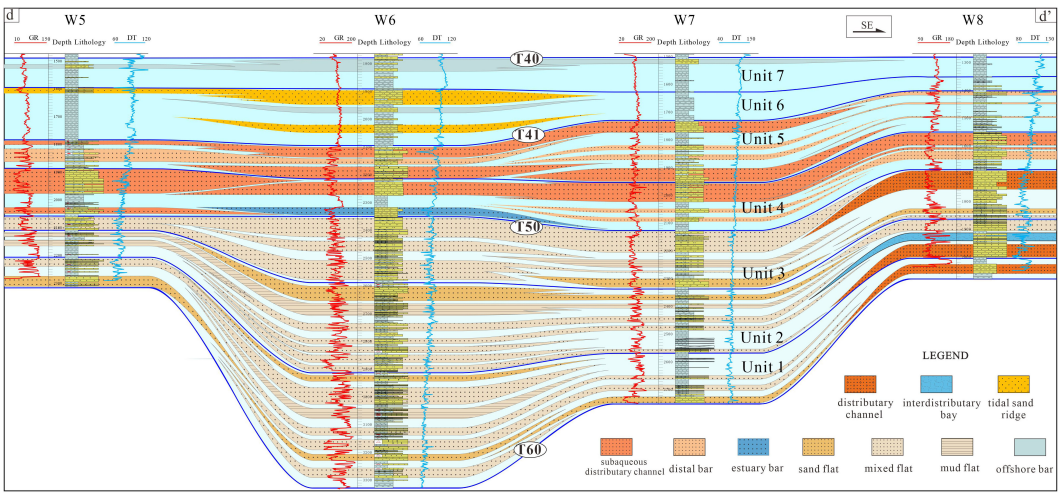


FIGURE 7
Stratigraphic correlation section from Well W5 to Well W8 showing the sedimentary architecture and depositional evolution process of the Miocene Zhujiang Formation. The well locations are shown in Figure 1B.

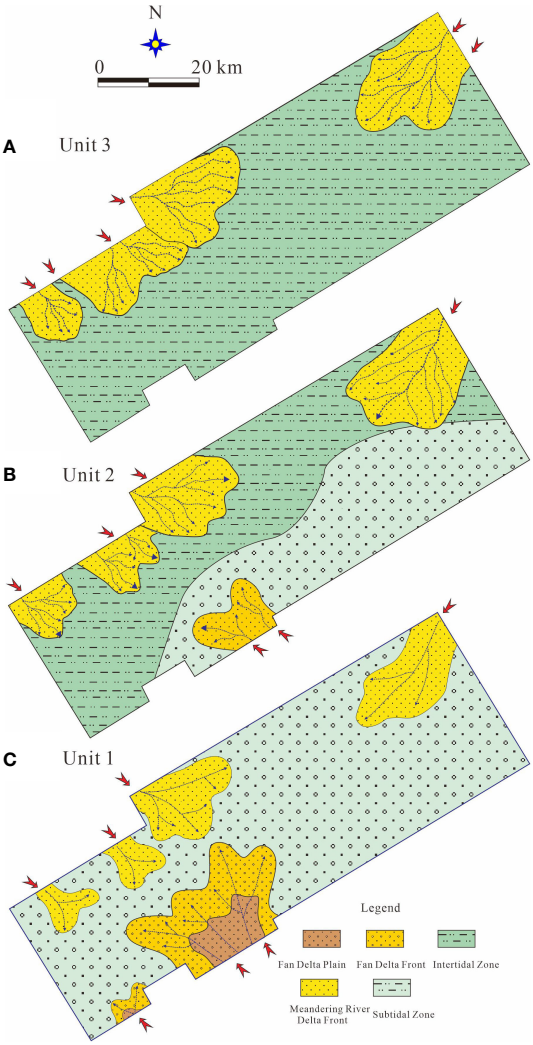


FIGURE 8
Planar distributions of depositional systems of Units 1-3 within the early Miocene Zhujiang Formation. **(A)** Distribution map of depositional systems of Unit 3. **(B)** Distribution map of depositional systems of Unit 2. **(C)** Distribution map of depositional systems of Unit 1.

bedded fine-grained sandstones and siltstones with a general upward coarsening pattern and parallel bedding, displaying a funnel gamma curve shape (Figures 6, 7). FA7 is characterized by thin bedded silty mudstones and siltstones interbedded with thin layers of mudstones, showing a medium funnel shape on the gramme curve (Figures 6, 7). It also exhibits ripple laminae, soft deformation structures, and horizontal bedding.

#### 4.1.3.2 Interpretation

The lithofacies associations of FA5-FA7 are interpreted as meandering river delta front deposits (Galloway, 1975; Orton and Reading, 1993; Zhang, 2019). FA5 represents subaqueous distributary channel deposits, which are commonly stacked vertically. It is dominated by vertical accretion rather than erosion Tian et al., 2021). FA6 indicates estuary bar deposits, which are vertically associated with FA5. FA7 is interpreted as distal bar deposits, and the mudstone layers indicate a relatively lenticular environment (Galloway, 1975; Orton and Reading, 1993).

#### 4.1.3.3 Distribution

Meandering river deltas were prevalent within the Zhujiang Formation, particularly in Units 4-5 (Figures 8, 9). The sediments for these meandering river deltas originated from the northwest and northeast, gradually filling the depression (Figures 8, 9). In seismic profiles, meandering river delta deposits are distinguished by their sheet-shaped seismic reflection configurations, medium to high amplitude, and strong continuity (Figures 3, 4). In stark contrast to the fan deltas located in the southern part of the depression, meandering river delta deposits exhibit a significantly finer grain size (Figures 6, 7). Delta front deposits were widely distributed and primarily consisted of subaqueous distributary channels, estuary bars and distal bars (Figures 8, 9).

### 4.1.4 Lithofacies associations FA8-FA10: tidal flat deposits

#### 4.1.4.1 Description

This group of lithofacies associations consists of FA8, FA9 and FA10. FA8 is composed of gray fine-grained sandstones with an average grain size of 0.25-0.4 mm, interbedded with cm-mm scale layers of dark gray mudstones to siltstones with a mean grain size of 0.06-0.23 mm (Figure 5). The thickness of a single layer of sandflat ranges from 3 mm to 2.2 cm, with an average of 7 mm (Figure 5). FA9 is characterized by interbedded thin layers of sandstones and mudstones, featuring tidal rhythmic bedding, ripple bedding, lenticular bedding, and bioturbation structures (Figure 5). FA10 mainly consists of thick layers of mudstones interbedded with thin layers of sandstones, displaying horizontal lamination and widespread strong bioturbation structures. In comparison to FA8, the sediments of FA10 were significantly finer, with a mean grain size of 0.03-0.12 mm (Figure 5).

#### 4.1.4.2 Interpretation

The lithofacies associations of FA8-FA10 are interpreted as tidal flat deposits (Wang et al., 2014; Zhang, 2019). FA8, with a high sandstone content (>70%), represents sandy flat deposits (Wang et al., 2014). FA9 is interpreted as mixed flat deposits, while FA10, with a high content of mudstone (>50%), represents mud flat deposits (Wang et al., 2014).

#### 4.1.4.3 Distribution

Tidal flat facies was the dominant depositional system in Units 1-3 (Figure 8). However, it disappeared in Units 4-7 due to subsequent marine regression. In seismic profiles, this facies is characterized by high to extremely high amplitude, strong continuity, and sheet-shaped seismic reflection configurations (Figures 3, 4). Tidal flat deposits exhibit significant zonation and consist of three facies associations: intertidal sandflat, subtidal sandflat, and subtidal mudflat (Figure 8). Sand flats were distributed in the sub-tidal zone and lower part of the intertidal zone, while mud flats occupied the upper parts of the intertidal zone and consisted mainly of dark gray mudstones (Figure 8).

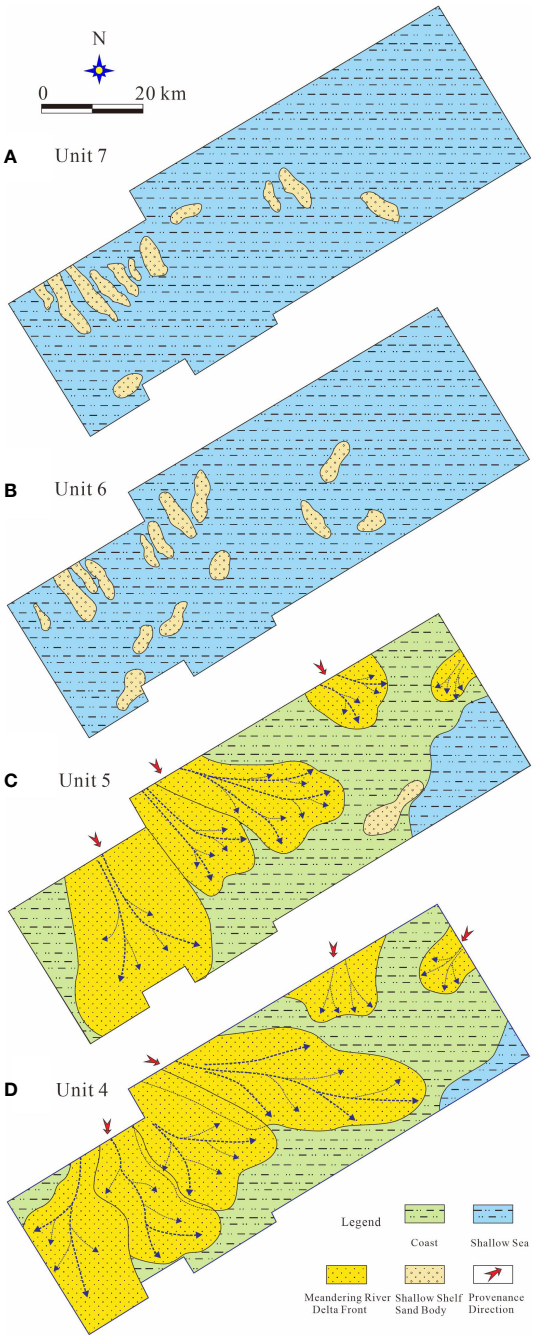


FIGURE 9
Planar distributions of depositional systems of Units 4-7 within the early Miocene Zhujiang Formation. **(A)** Distribution map of depositional systems of Unit 7. **(B)** Distribution map of depositional systems of Unit 6. **(C)** Distribution map of depositional systems of Unit 5. **(D)** Distribution map of depositional systems of Unit 4.

### 4.1.5 Lithofacies associations FA11-FA12: shallow marine shelf sand bodies

#### 4.1.5.1 Description

The lithofacies associations of FA11 and FA12 are characterized by distinct features. FA11 is mainly composed of gray fine sandstones, featuring fishbone-shaped cross bedding and wavy bedding (Figure 5). The gamma curve presents a bimodal box or bell-shaped pattern, and displays low-frequency strong amplitude lens-shaped reflections in the seismic section (Figures 6, 7). FA12 is primarily composed of grayish-white muddy sandstones interbedded with mudstones, exhibiting an upward coarsening pattern and commonly developed lens-shaped and ripple cross-bedding (Figure 5). It is characterized by a funnel shape with high natural gamma values on the natural gamma ray curve, and appears as medium frequency, medium amplitude sheet-like reflections in the seismic profile (Figures 3, 6, 7).

#### 4.1.5.2 Interpretation

FA11-FA12 are interpreted as shallow marine shelf sand deposits. FA11 is interpreted as tidal sand ridge deposits, formed by the unloading of sediment carried by tidal currents (Bassetti et al., 2006; Zhang, 2019). FA12 represents offshore bar deposits, formed by the erosion, transport, and deposition of early sediments by waves and alongshore currents (Bassetti et al., 2006; Zhang, 2019).

#### 4.1.5.3 Distribution

Shallow marine shelf sand deposits were distributed in Units 6-7 (Figure 9). They developed near ancient uplifts, such as the Qionghai Uplift and the Shenhu Uplift. These deposits exhibit good physical properties, making them favorable sedimentary facies for hydrocarbon accumulation.

### 4.1.6 Lithofacies association FA13: coastal-shallow marine shelf deposits

#### 4.1.6.1 Description

FA13 mainly consists of thick-bedded gray to black mudstones with interbedded thin layer of siltstones and horizontal bedding, with the thickness of a single layer varying between 3 m and 52 m (Figures 5, 6). In seismic profiles, it is characterized by a continuous flat reflection pattern and low to high amplitude (Figures 3, 4).

#### 4.1.6.2 Interpretation

FA13 is interpreted as coastal-shallow marine shelf deposits (Zhang, 2019). The interbedded siltstones are interpreted as deposits from meandering river delta formations (Figures 5, 6).

#### 4.1.6.3 Distribution

The coastal-shallow marine shelf deposits can be divided into two types: the coastal mudstone deposits and the shallow marine shelf mudstone deposits. The coastal mudstone deposits were mainly developed in Units 4-5, with a larger range in Unit 4 than in Unit 5 (Figure 9). The shallow marine shelf mudstone deposits were mainly developed in Units 6 and 7, with their ranges gradually expanding from Unit 6 to Unit 7 (Figure 9).

## 4.2 Distribution of depositional systems in different depositional units

### 4.2.1 Unit 1

During the sedimentary period of Unit 1, a variety of depositional systems were formed in the study area, including

tidal flats, fan deltas, and meandering river deltas (Figure 8). The dominant depositional environment was the tidal flat. Subtidal sediments were widely distributed, mainly composed of subtidal sand and mud flats. Fan deltas were found only in the northern region, positioned at the footwall of the Zhusannan Fault (Figure 8). Meandering river deltas were observed in the northwest and eastern parts of the study area, with only delta fronts present (Figure 8).

#### 4.2.2 Unit 2

Unit 2 exhibited similar characteristics to Unit 1, with the presence of tidal flats, fan deltas, and meandering river deltas in the study area (Figure 8). However, the range of fan deltas was significantly smaller, while that of meandering river deltas was larger (Figure 8).

#### 4.2.3 Unit 3

During the depositional period of Unit 3, tidal flats and meandering river deltas were formed in the study area, with the tidal flat being the dominant depositional environment (Figure 8). Fan deltas no longer developed in the study area, which is a stark contrast to Unit 2, indicating the disappearance of the southern source (Figure 8). The ranges of meandering river deltas in Unit 3 were slightly larger compared to those in Unit 2 (Figure 8).

#### 4.2.4 Unit 4

During the depositional period of Unit 3, the predominant depositional environment in the study area shifted from the tidal flats to meandering river deltas (Figure 9). The meandering river deltas originating from the northwest experienced substantial expansion, now encompassing over half of the study area (Figure 9). Notably, this expansion led to the formation of thick layers of subaqueous distributary channels, which represent the most significant feature of Unit 4 (Figure 9). In contrast, the meandering river delta sourced from the west exhibited a more restricted range (Figure 9).

#### 4.2.5 Unit 5

Unit 5 acquired the depositional traits of Unit 4, with the prevailing depositional environment being meandering river deltas (Figure 9). The extent of the meandering river deltas experienced a considerable reduction, whereas the coverage of the shallow marine shelf expanded (Figure 9). These modifications align perfectly with the swift increase in sea level. Furthermore, small-scale offshore bars were detected in the southern region.

#### 4.2.6 Unit 6

Unit 6 represented a noticeable change in the depositional systems observed in the study area. The depositional environment shifted from a coastal environment in Units 4-5 to the shallow marine shelf system in Unit 6 (Figure 9). The meandering river deltas that originated from the northwest were no longer present in the study area, being replaced by thick layers of marine mudstones (Figures 6, 7). In the adjacent regions of the Qionghai Uplift and Shenhu Uplift, there were shallow marine shelf sand bodies on the continental shelf (Figure 9). These sand bodies consisted of storm sands, tidal sand ridges, and offshore sand bars (Figures 6, 7). Additionally, the range of meandering river delta originating from the west expanded, indicating an increased input of sediment from the Pearl River source (Figure 9).

#### 4.2.7 Unit 7

Similar depositional characteristics were observed in Unit 7 as in Unit 6, with the predominant depositional environment being the shallow marine shelf system (Figure 9). The deposition of sand-rich systems was primarily contributed by shallow continental shelf sand bodies and meandering river deltas (Figure 9). The meandering river delta originating from the west continued to expand (Figure 9).

## 5 Discussion

### 5.1 The observation of long-term Miocene marine transgression in the PRMB

The Miocene period witnessed a global marine transgression event, which was observed in various regions, such as South America. Along the South American east coast, a long-term period of sea level fall between 25 Ma and 18 Ma is proposed, followed by another fall between 18 and 13 Ma (Mörner, 2004). During the early Miocene, southern Argentina and Chile were submerged by this long-term marine transgression. A contemporaneous marine transgression was also observed in northern Argentina (Bechis et al., 2014). Generally, the Miocene marine transgression can be divided into two phases: one in the late Oligocene-early Miocene and the other in the late Miocene (Rossetti et al., 2013). The early Miocene transgression is marked by the most widespread transgression, which is consistent with a global sea level lowstand during this period (Haq et al., 1987; Miller et al., 2005).

In the PRMB, a long-term marine transgression was observed during the sedimentary period of the early Miocene Zhujiang Formation. The locations of coastal onlap points in Figure 4 continued to rise, indicating a rapid increase in relative sea level in the PRMB. During the early Miocene (23.8 Ma), the Qionghai Uplift was exposed to the water surface and underwent minimal erosion (Figure 4). The dominant depositional facies during this period in the study area were fan deltas and tidal flats, with exposed fan delta plain deposits visible in the drilling cores (Figures 5–7). The shoreline was situated in the southern region of the Shenhu Uplift during this time (Figure 3), suggesting an extremely low sea level (< 10 m) in the early Miocene in the PRMB. Subsequently, the Qionghai Uplift submerged, initiating the marine transgression (Figure 4). The shoreline moved northwards during the sedimentary period of Unit 4, and large-scale delta fronts were deposited in the PRMB, indicating a rapid transgression process (Figure 9). The depositional system changed from a coastal to a shallow sea environment during the deposition of Units 6-7, indicating a continued rise in sea level (Figure 9). More importantly, the abundance and diversity of benthic foraminifera show a notable rise in the presence of *Uvigerina*, *Lenticulina*, and *Martinottiella* in the Zhujiang Formation (Figure 10), suggesting a gradual rise in sea level (Mao et al., 2019). According to the quantitative relationship between the percentage content of benthic foraminifera

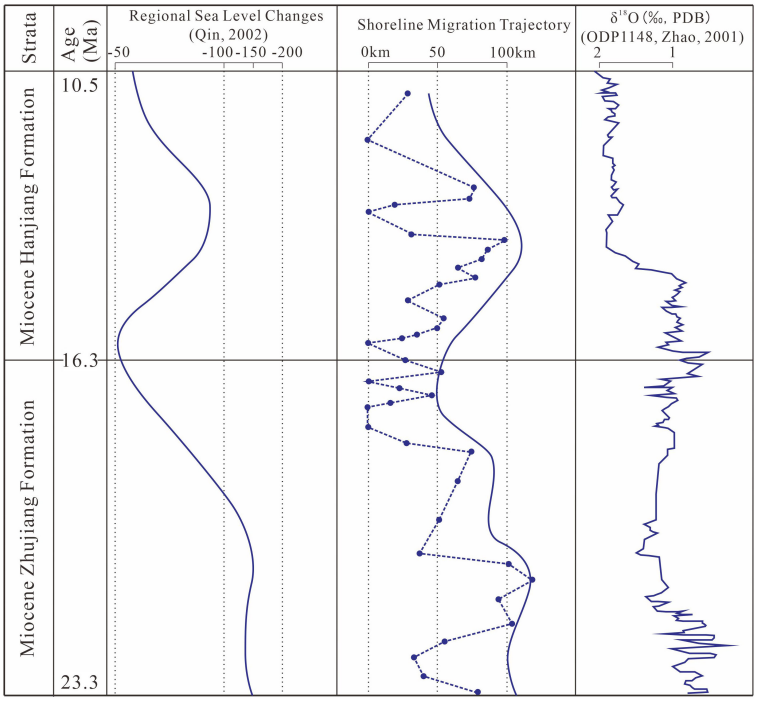


FIGURE 10
Map showing the regional sea level changes in the PRMB. The regional sea level curve is from Qin, 2002 and Mao et al. (2019), and $\delta^{18}O$ data is from ODP 1148 (Zhao et al., 2001). The shoreline migration trajectory is from Zhang, 2019.

and ancient water depth described by Mao et al. (2019), the paleo-water depth in the late depositional period of Zhujiang Formation was estimated around 170 m (Mao et al., 2019), which aligns with a depositional background characteristic of shallow to outer-shallow marine environments. Therefore, this study suggests that the early Miocene Zhujiang Formation corresponds to a significant period of transgressive events in the South China Sea, ultimately leading to a sea-level increase of at least 100 m (Figure 10).

The observation of long-term Miocene marine transgression in the PRMB is further substantiated by the changes in relative sea level in the PRMB (Qin, 2002) (Figure 10). Qin (2002) and Mao et al. (2019) demonstrate that the average sea level of the PRMB rose by at least 100 m during the deposition period of the Zhujiang Formation. This is consistent with the rapidly rising trend observed in global sea level changes in Haq et al. (1987), although there are some differences in the details of sea level fluctuations (Figure 10). The regional sea level demonstrates a rapidly rising trend between 21 Ma and 16.3 Ma, and the shoreline and deltaic depositional systems rapidly retreated landwards, representing a rapid marine transgression (Zhang, 2019) (Figure 10). Subsequently, the regional sea level reached its peak around 16.3 Ma, corresponding to the location of maximum marine transgression revealed by long-term shoreline migration tracks (Zhang, 2019) (Figure 10). The early Miocene $\delta^{18}O$ increase of benthic foraminifera suggests that this long-term marine transgression is associated with a significant expansion of the Antarctic ice sheet (Zhao et al., 2001), suggesting it was genetically controlled by global climatic changes.

It is important to note that this long-term Miocene marine transgression does not mean a continuous rise in sea level, but rather a general upward trend in the overall sea level (Rossetti et al., 2013). This upward trend includes complex short-term fluctuations in sea level (Rossetti et al., 2013).

## 5.2 Depositional evolution in response to marine transgression in the PRMB

This study reveals the complexity of depositional evolution with the presence of four different types of depositional systems, which are closely related to the marine transgression process (Figures 8, 9). During the early Miocene marine transgression in the PRMB, the primary depositional system type underwent a remarkable shift (Figures 8, 9). The evolutionary process of depositional systems can be divided into three stages, including the early stage (Units 1-3), the middle stage (Units 4-5), and the late stage (Units 6-7). In the early stage, Units 1-3 featured a predominant tidal flat environment, which then transitioned into meandering river deltas in the middle stage (Units 4-5) (Figures 8, 9). Finally, in the late stage (Units 6-7), it evolved into a shallow marine shelf system. It can be concluded that the dominant depositional system type evolved from tidal flat in Units 1-3 to meandering river delta in Units 4-5, and finally to shallow marine shelf system in Units 6-7 (Figures 8, 9). This evolutionary progression was intricately tied to the overarching process of marine transgression. The water depth of tidal flat deposits in Units 1-3 was usually less than 10 m, while that of shallow marine shelf systems in Units 6-7 varied between 150 m and 200 m (Mao et al., 2019). These changing water depths further underscore the dynamic nature of marine transgression. Furthermore, shifts in sub-facies types also provide key insights into the

unfolding marine transgression. As an illustration, the dominant depositional facies transformed from the intertidal zone in Unit 1 to the subtidal zone in Unit 3, a clear reflection of the rising sea level.

The Miocene marine transgression profoundly impacted the distribution patterns of depositional systems. As Unit 1 transitioned into Unit 5, we observed a gradual reduction in the deposition of proximal fan deltas originating from nearby uplifts, while the extent of distal meandering river deltas gradually expanded (Figures 8, 9). Subsequently, throughout the depositional stages of Units 6-7, the entire study area underwent a notable transformation as deltas disappeared, giving way to the dominance of shallow marine mudstone sedimentation (Figures 8, 9). This transformation aligns with the provenance evolution history reconstructed by zircon U-Pb geochronology and heavy mineral composition in the PRMB (e.g., Shao et al., 2016; Liu et al., 2022a). Liu et al. (2022a) suggested a significant shift in the source to sink system occurring in the early Miocene in the PRMB. The Eocene-Oligocene sediments display similar age patterns ranging from 100 Ma to 450 Ma, indicating that they were derived from nearby Shenhu and Qionghai Uplifts (Liu et al., 2022a). By contrast, the upper Zhujiang Formation sediments are marked by a significant increase of Paleozoic and Precambrian zircons, displaying similar age patterns to the sediments in the Pearl River (Liu et al., 2022a). This suggests that the upper Zhujiang Formation sediments were mainly derived from South China Block via the Pearl River system. During the depositional period of Zhujiang Formation, the contribution of nearby sources steadily decreased, while long-distance transported sediments from the South China Block gradually increased (Liu et al., 2022a) (Figures 8, 9). It is important to note that in the late stage (Units 6-7), deltaic deposits ceased to form within the study area, with only shallow marine mudstone deposition developed (Figure 9). The absence of deltaic deposits in the study area should be attributed to the ongoing marine transgression, resulting in deltas retreat from the study area. Likely, the deltaic deposits were situated outside the study area in this period, particularly to the north.

In addition to marine transgression, the depositional evolution in the PRMB was significantly influenced by sediment supply and paleo-geomorphology. During the deposition of the Zhujiang Formation, the sediment supply rate exhibited non-uniformity (Wang et al., 2021; Liu et al., 2022b), as evidenced by variations in the sandstone percentage in drilling cores. For instance, when compared to Unit 4, the sedimentation rate in meandering river deltas notably decreased, leading to a reduction in the sandstone percentage from 65% to 40% (Figures 6, 7). These findings align well with previous research conclusions in Liu et al. (2022b). In addition, paleo-geomorphology played a pivotal role in the spatial distribution of the deposition system (Liu et al., 2014; Xie et al., 2014; Wang et al., 2021). Notably, the paleo-geomorphic landscape underwent substantial changes during the deposition period of the Miocene Zhujiang Formation (Figure 11). In the early stage, the basin displayed distinct uplifts and depressions, with the elevated regions acting as sources through erosion,

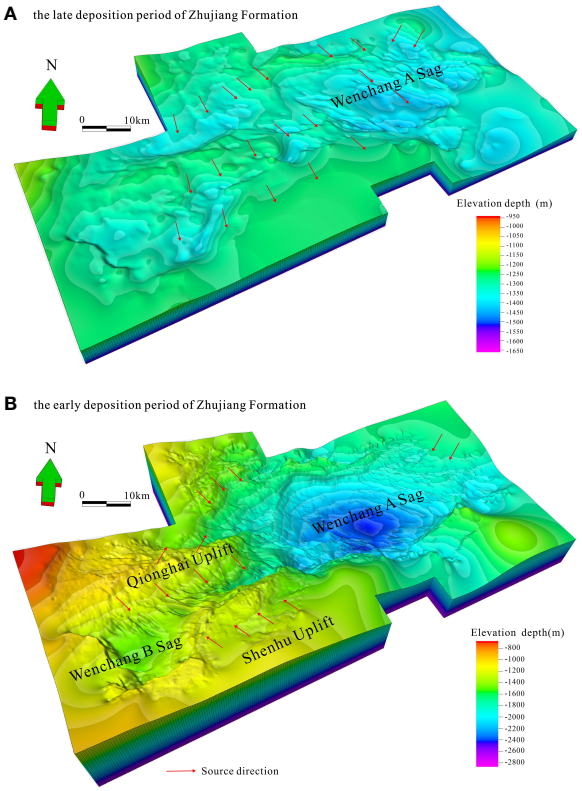


FIGURE 11
The palaeogeographic maps of Horizons T40 (the top boundary of the Zhujiang Formation) and T60 (the bottom boundary of the Zhujiang Formation), showing the difference in geomorphic features. **(A)** The palaeogeographic map of Horizon T40. **(B)** The palaeogeographic map of Horizon T60.

contributing to the development of small-scale fan delta deposits (Figures 11, 12). By contrast, in the late stage, the pattern of uplifts and depressions in the basin significantly diminished, and the deposition of proximal sources ceased. During this period, the Qionghai Uplift submerged, ceasing to serve as a source and instead becoming a submerged, restricted highland (Figures 11, 12). The sand bodies previously formed through tidal action upon the existing sediments within the uplifted area subsequently transformed into shallow marine shelf sand bodies. This formation process elucidates the enrichment of shallow marine shelf sand bodies around the Qionghai Uplift development region.

## 5.3 Sedimentological and exploration significance

This study presents a valuable opportunity to enhance our comprehension of the depositional evolution occurring during the long-term marine transgression from 23.3 Ma to 16.3 Ma. The findings of this study shed light on the following characteristics of the depositional system during the transgression process: (1) The continuous transgression process not only results in alterations in the extent of distribution of depositional systems but also noteworthy modifications in sediment types, thereby leading to increased complexity in the depositional system (Figure 12). (2) In the initial phase of transgression, characterized by low sea levels, intertidal flats predominantly govern the depositional systems (Figures 8, 12). (3) As the transgression persists, there are significant changes in paleogeography and provenance directions, consequently weakening the supply from nearby sources and intensifying the supply from distant sources (Figures 9, 12). (4) When the sea level reaches a certain depth, the deposition of shallow marine mudstone becomes prevalent (Figure 12). These sedimentary features exhibit substantial disparities from the depositional evolution process observed during short-period transgressions (e.g., Zhou et al., 2014; Tang et al., 2018; Zhang et al., 2023), which primarily impact the distribution of depositional systems rather than their types.

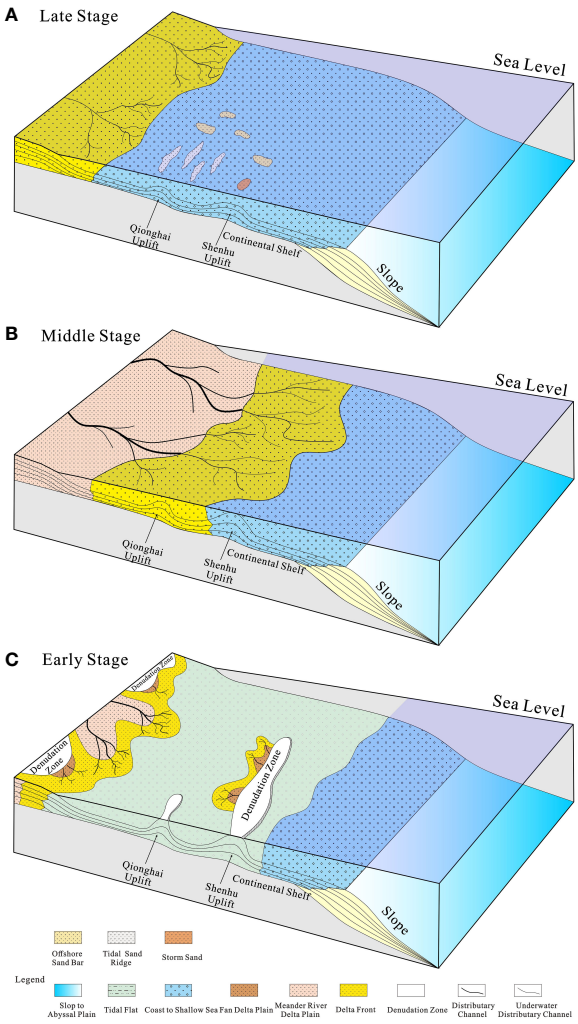


FIGURE 12
The three-stage depositional model showing the evolution process in response to marine transgression in the PRMB. It can be divided into three stages: **(A)** the late stage; **(B)** the middle stage; and **(C)** the early stage.

The marine transgression significantly influenced the depositional evolution, thereby impacting the distribution of hydrocarbon resources and the types of traps in the PRMB (Huang et al., 2003; Xie et al., 2021; Wu, 2022). Oil and gas reserves in the PRMB originated from the underlying Wenchang and Enping source rocks (Toc = 1.6~2.5%, HI = 233-332 mg/g TOC) (Quan et al., 2020; Fu et al., 2022; Yang et al., 2022). These hydrocarbons migrated from the deep lake through syn-sedimentary faults to the Qionghai Uplift. In the earlier Units 1-3, two types of traps were identified: up-dip wedge-out traps and fault traps (Figure 13). Up-dip wedge-out traps predominantly formed in the relatively elevated structural areas near the Qionghai Uplift (Wu, 2022) (Figure 13). In Units 4-5, in addition to the up-dip wedge-out and fault traps, stratigraphic onlap traps were observed at the top of the Qionghai Uplift (Figure 13).

Units 6-7 exhibited a different geological characteristic as shallow marine shelf sand bodies were prevalent, favoring the development of lithologic lenticular traps (Figure 13). The development of shallow marine shelf sand bodies is primarily influenced by several factors including geomorphology, sea level fluctuations, and sediment supply (Liu et al., 2022b). When marine transgression occurred, pre-existing sand bodies located in high geomorphic units were reworked by hydrodynamic conditions such as tidal currents and storm waves (Liu et al., 2022b). The scale and distribution of these sand bodies are further influenced by sediment supply. This formation process helps explain why shallow-sea shelf sand bodies are primarily located near the Qionghai and Shenhu Uplifts during periods of high sea level. These shallow marine shelf sand bodies have garnered significant attention for future exploration due to their high-quality reservoir properties, with average porosity and permeability values exceeding 18% and 140 mD, respectively (Liu et al., 2022b). Furthermore, compared to other types of traps, hydrocarbon exploration in the shallow marine shelf sand bodies presents fewer challenges. These advantages, including shallow burial, lower exploration costs, and good seismic data quality, have a profound impact on hydrocarbon enrichment and increase the success rate of hydrocarbon exploration in the region.

## 6 Conclusions

(1) A long-term marine transgression occurred between 23.3 Ma and 16.3 Ma in the Pearl River Mouth Basin, northern South China Sea, resulting in at least a 100 m rise in relative sea level.

(2) Within the early Miocene Zhujiang Formation, we have recognized thirteen types of lithofacies associations and identified four distinct depositional facies including tidal flats, fan deltas, meandering river deltas, and shallow marine shelf sand bodies. The progression of the marine transgression led to a significant shift in the types of depositional systems, transitioning from tidal flats in Units 1-3 to meandering river deltas in Units 4-5, and ultimately evolving into shallow marine shelf systems in Units 6-7.

(3) In the early stage (Units 1-3), the regional uplifts hindered sea level transgression and caused erosion, leading to the development of small-scale proximal fan deltas. In the middle stage (Units 4-5), these regional uplifts submerged, and meandering river deltas dominated with sediments derived from distant extrabasinal sources. During the late stage (Units 6-7), regional sea levels reached their peak, transforming the entire basin into a shallow marine shelf system.

(4) Our study highlights that the long-term transgression process not only alters the distribution of depositional systems but also leads to noteworthy modifications in sediment types, resulting in increased complexity in depositional systems. Furthermore, this marine

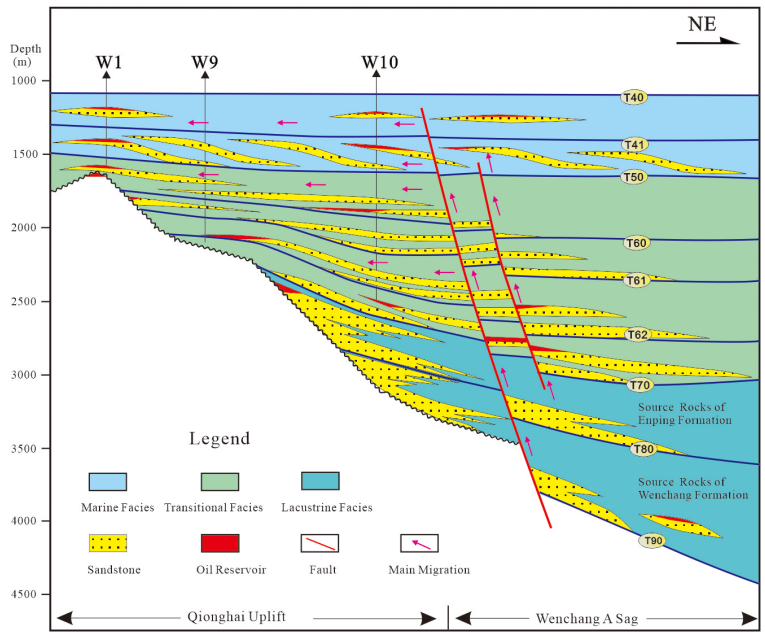


FIGURE 13
The type and distribution of oil and gas reservoirs across the representative section in the Zhu III Depression, PRMB.

transgression has a significant impact on the distribution of hydrocarbon resources and trap types. The shallow marine shelf sand bodies in Units 6-7 are recommended as the key targets for future exploration.

## Data availability statement

The original contributions presented in the study are included in the article/supplementary material. Further inquiries can be directed to the corresponding author.

## Author contributions

EL: Conceptualization, Funding acquisition, Investigation, Resources, Writing – original draft. WL: Data curation, Project administration, Resources, Writing – review & editing. DY: Project administration, Supervision, Validation, Writing – review & editing. YD: Project administration, Writing – review & editing. SC: Formal Analysis, Visualization, Writing – original draft. JZ: Data curation, Software, Writing – original draft. YJ: Data curation, Software, Writing – original draft.

## Funding

The author(s) declare financial support was received for the research, authorship, and/or publication of this article. This work was supported by the National Natural Science Foundation of China (Nos.42072142, 41702121).

## Acknowledgments

We gratefully acknowledge the editor for careful editorial handling.

## Conflict of interest

Authors WL and YD are employed by China National Offshore Oil Corporation.

The remaining authors declare that the research was conducted in the absence of any commercial or financial relationships that could be construed as a potential conflict of interest.

## Publisher's note

All claims expressed in this article are solely those of the authors and do not necessarily represent those of their affiliated organizations, or those of the publisher, the editors and the reviewers. Any product that may be evaluated in this article, or claim that may be made by its manufacturer, is not guaranteed or endorsed by the publisher.

## References

Andrés, G. D., Salvador, A., Susana, G. S., Gabriela, V. L., and Osvaldo, S. J. (2011). Evolution of a coastal alluvial deposit in response to the last quaternary marine transgression, Bahía Blanca estuary, Argentina. *Quat. Res.* 75, 614–623. doi: 10.1016/j.yqres.2010.12.006

Bassetti, M. A., Jouet, G., Dufois, F., Berné, S., Rabineau, M., and Taviani, M. (2006). Sand bodies at the shelf edge in the Gulf of Lions (Western Mediterranean): Deglacial history and modern processes. *Mar. Geol.* 234, 93–109. doi: 10.1016/j.margeo.2006.09.010

Bechis, F., Encinas, A., Concheyro, A., Litvak, V. D., Aguirre-Urreta, B., and Ramos, V. A. (2014). New age constraints for the Cenozoic marine transgressions of northwestern Patagonia, Argentina (41°-43°S): Paleogeographic and tectonic implications. *J. South Am. Earth Sci.* 52, 72–93. doi: 10.1016/j.jsames.2014.02.003

Bogemans, F., Roe, H. M., and Baeteman, C. (2016). Incised pleistocene valleys in the Western Belgium coastal plain: age, origins and implications for the evolution of the Southern North Sea Basin. *Palaeogeogr. Palaeoclimatol. Palaeoecol.* 456, 46–59. doi: 10.1016/j.palaeo.2016.04.047

Choi, S. J., Merritts, D. J., and Ota, Y. (2008). Elevations and ages of marine terraces and late quaternary rock uplift in southeastern Korea. *J. Geophys. Res.* 113, B10403. doi: 10.1029/2007JB005260

Clift, P. D., Brune, S., and Quinteros, J. (2015). Climate changes control offshore crustal structure at South China Sea continental margin. *Earth Planet. Sci. Lett.* 420, 66–72. doi: 10.1016/j.epsl.2015.03.032

Coleman, J. M., and Wright, L. D. (1975). "Modern river deltas: variability of processes and sand bodies," in *Deltas: models for exploration*. Ed. M. L. Broussard (Houston: Houston Geological Society), 99–149.

Franke, D. (2013). Rifting lithosphere breakup and volcanism: comparison of magma-poor and volcanic rifted margins. *Mar. Petrol. Geol.* 43, 63–87. doi: 10.1016/j.marpetgeo.2012.11.003

Fu, C., Huang, W. S., Li, S. L., and Chen, H. P. (2019). The spatial discrepancy of Miocene transgression and its corresponding channel transformation pattern: A case study of the carabobo region in the northeast Venezuela basin. *J. South Am. Earth Sci.* 89, 347–365. doi: 10.1016/j.jsames.2018.11.019

Fu, X. Y., Chen, S. J., You, J. J., Li, H., and Lei, M. Z. (2022). Geochemical characteristics and sources of crude oil in the Wenchang B depression and the Western Qionghai uplift of the Zhu-3 sub-basin, Pearl River Mouth Basin, South China Sea. *J. Pet. Sci. Eng.* 219, 111091. doi: 10.1016/j.petrol.2022.111091

Galloway, W. E. (1975). "Process framework for describing the morphologic and stratigraphic evolution of deltaic depositional systems," in *Deltas: models for exploration*. Ed. M. L. Broussard (Houston: Houston Geological Society), 87–98.

Ge, J. W., Zhao, X. M., Tan, M. X., Zhuo, H. T., Liu, C. S., and Jones, B. G. (2022). Sequence stratigraphy and depositional evolution of the north-eastern shelf (33.9–10.5 Ma) of the Pearl River Mouth Basin, South China Sea. *Mar. Pet. Geol.* 141, 105697. doi: 10.1016/j.marpetgeo.2022.105697

Guo, X. S., Fan, N., Liu, Y. H., Liu, X. L., Wang, Z. K., Xie, X. T., et al. (2023a). Deep seabed mining: Frontiers in engineering geology and environment. *Int. J. Coal Sci. Technol.* 10, 23. doi: 10.1007/s40789-023-00580-x

Guo, X. S., Liu, X. L., Li, M. Q., and Lu, Y. (2023b). Lateral force on buried pipelines caused by seabed slides using a CFD method with a shear interface weakening model. *Ocean Eng.* 280, 114663. doi: 10.1016/j.oceaneng.2023.114663

Haq, B. U., Hardenbol, J., and Vail, P. R. (1987). Chronology of fluctuating sea levels since the Triassic. *Science* 235, 1156–1167. doi: 10.1126/science.235.4793.1156

Hayes, D. E., and Nissen, S. S. (2005). The South China Sea margins: implications for rifting contrasts. *Earth Planet. Sci. Lett.* 237, 601–616. doi: 10.1016/j.epsl.2005.06.017

Huang, B., Xiao, X., and Zhang, M. (2003). Geochemistry grouping and origins of crude oils in the western Pearl River Mouth Basin, offshore South China Sea. *Org. Geochem.* 34, 993–1008. doi: 10.1016/S0146-6380(03)00035-4

Li, Y., Tsukamoto, S., Shang, Z. W., Tamura, T., Wang, H., and Frechen, M. (2019). Constraining the transgression history in the Bohai Coast China since the Middle Pleistocene by luminescence dating. *Mar. Geol.* 416, 105980. doi: 10.1016/j.margeo.2019.105980

Liu, E. T., Chen, S., Yan, D. T., Deng, Y., Wang, H., Jing, Z. H., et al. (2022a). Detrital zircon geochronology and heavy mineral composition constraints on provenance evolution in the Western Pearl River Mouth Basin, northern South China Sea: A

source to sink approach. *Mar. Petrol. Geol.* 145, 105884. doi: 10.1016/j.marpetgeo.2022.105884

Liu, E. T., Deng, Y., Lin, X. D., Yan, D. T., Chen, S., and Shi, X. B. (2022b). Cenozoic depositional evolution and stratal patterns in the western Pearl River Mouth Basin, South China Sea. *Energies* 15 (21), 8050. doi: 10.3390/en15218050

Liu, J., Saito, Y., Wang, H., Zhou, L., and Yang, Z. (2009). Stratigraphic development during the late pleistocene and holocene offshore of the Yellow River delta, Bohai Sea. *J. Asian Earth Sci.* 36, 318–331. doi: 10.1016/j.jseaes.2009.06.007

Liu, E. T., Wang, H., Li, Y., Zhou, W., Leonard, N. D., Lin, Z. L., et al. (2014). Sedimentary characteristics and tectonic setting of sublacustrine fans in a half-graben rift depression, Beibuwan Basin, South China Sea. *Mar. Petrol. Geol.* 52, 9–21. doi: 10.1016/j.marpetgeo.2014.01.008

Mao, X. L., Xu, S. L., and Liu, X. Y. (2019). Late Cenozoic high resolution biostratigraphy and its bearing on sea-level fluctuation in the western Pearl River Mouth Basin. *Mar. Geol. Quat. Geol.* 39 (3), 40–50. doi: 10.16562/j.cnki.0256-1492.2017081601

Miller, K. G., Kominz, M. A., Browining, J. V., Weight, J. D., Mountan, G. S., Sugarman, P. J., et al. (2005). The phanerozoic record of global sea-level change. *Science* 310, 1293–1298. doi: 10.1126/science.1116412

Mörner, N. A. (2004). Estimating future sea level changes from past records. Global Planet. Change 40, 49-54. doi: 10.1016/S0921-8181(03)00097-3

Müller, R. D., Sdrolias, M., Gaina, C., Steinberger, B., and Heine, C. (2008). Long-term sea-level fluctuations driven by ocean basin dynamics. *Science* 319, 1357–1362. doi: 10.1126/sci.1151540

Orton, G. J., and Reading, H. G. (1993). Variability of deltaic processes in terms of sediment supply, with particular emphasis on grain size. *Sedimentology* 40, 475–512. doi: 10.1111/j.1365-3091.1993.tb01347.x

Poisson, A., Vrielynck, B., Wernli, R., Negri, A., Bassetti, M. A., Büyükmeriç, Y., et al. (2016). Miocene transgression in the central and eastern parts of the Sivas Basin (Central Anatolia, Turkey) and the cenozoic palaeogeographical evolution. *Int. J. Earth. Sci.* 105, 339–368. doi: 10.1007/s00531-015-1248-1

Qin, G. Q. (2002). Late Cenozoic sequence stratigraphy and sea-level changes in Pearl River Mouth Basin, South China Sea. *China Offshore Oil Gas (Geology)* 16 (1), 1–10. doi: 10.16562/j.cnki.0256-1492.1996.04.001

Quan, Y. B., Liu, J. Z., Hao, F., Cai, Z. X., and Xie, Y. H. (2020). Paleosalinity assessment and its influence on source rock deposition in the Western Pearl River Mouth Basin, South China Sea. *Geol. Soc Am. Bull.* 132, 1741–1755. doi: 10.1130/B35319.1

Quan, Y., Liu, J., Zhao, D., Hao, F., Wang, Z., and Tian, J. (2015). The origin and distribution of crude oil in Zhu III sub-basin, Pearl River Mouth Basin. China. *Mar. Petrol. Geol.* 66, 732–747. doi: 10.1016/j.marpetgeo.2015.07.015

Rossetti, D. F., Bezerra, F. H. R., and Dominguez, J. M. L. (2013). Late Oligocene–Miocene transgressions along the equatorial and eastern margins of Brazil. *Earth-Sci Rev.* 123, 87–112. doi: 10.1016/j.earscirev.2013.04.005

Shanley, K. W., and McCabe, P. J. (1994). Perspectives on the sequence stratigraphy of continental strata. *AAPG Bull.* 78, 544–568. doi: 10.1306/BDFF9258-1718-11D7-8645000102C1865D

Shao, L., Qiao, P. J., Zhao, M., Li, Q. Y., Wu, M., Pang, X., et al. (2016). Depositional characteristics of the northern South China Sea in response to the evolution of the Pearl River. *Geol. Soc London Spec. Publ.* 429, 31–44. doi: 10.1144/SP429.2

Tang, Y. J., Zheng, Z., Chen, C., Wang, M. Y., and Chen, B. S. (2018). Evolution of the Lian River coastal basin in response to quaternary marine transgressions in Southeast China. *Sediment. Geol.* 366, 1–13. doi: 10.1016/j.sedgeo.2018.01.003

Tian, H. X., Lin, C. S., Zhang, Z. T., Li, H., Zhang, B., Zhang, M. L., et al. (2021). Depositional architecture, evolution and controlling factors of the Miocene submarine canyon system in the Pearl River Mouth Basin, northern South China Sea. *Mar. Petrol. Geol.* 128, 104990. doi: 10.1016/j.marpetgeo.2021.104990

Wang, H., Chen, S., Liu, E. T., He, J., Gan, H. J., Meng, F. L., et al. (2022). Typical gravity flow sedimentary features and provenance system in Yinggehai-Qiongdongnan Basin, northern South China Sea. *Bull. Geol. Sci. Technol.* 41 (5), 5–18. doi: 10.19509/j.cnki.dzkq.2022.0245

Wang, C., Liang, X. Q., Foster, D. A., Tong, C. X., Liu, P., Liang, X. R., et al. (2018). Linking source and sink: detrital zircon provenance record of drainage systems in Vietnam and the Yinggehai-Song Hong basin, South China Sea. *Geol. Soc Am. Bull.* 131, 191–204. doi: 10.1130/B32007.1

Wang, Y. R., Lin, C. S., Zhang, Z. T., Zhang, B., and Liu, H. Y. (2021). Sedimentary evolution and controlling factors of Early-Mid Miocene Deltaic systems in the Northern Pearl River Mouth Basin, south China Sea. *Sci. Rep.* 11 (1), 6134. doi: 10.1038/s41598-021-85369-1

Wang, Z. B., Yang, S. Y., Wang, Q., Zhang, Z. X., Zhang, X. H., Lan, X. H., et al. (2014). Late quaternary stratigraphic evolution on the outer shelf of the East China Sea. *Cont. Shelf Res.* 90, 5–16. doi: 10.1016/j.csr.2014.04.015

Wang, Y. Y., Zhao, Y. H., Ding, W. W., Fang, P. G., and Li, J. B. (2022). Cenozoic propagated rifting in the dangerous grounds in response to the episodic seafloor spreading of the South China Sea. *J. Earth. Sci.* 33 (4), 1031–1046. doi: 10.1007/s12583-020-1064-9

Wu, J. (2022). Key factors of far-source hydrocarbon enrichment in the northern uplift area of Enping Sag in Pearl River Mouth Basin. *Bull. Geol. Sci. Technol.* 41 (4), 117–124. doi: 10.19509/j.cnki.dzkq.2022.0020

Xie, G. J., Chen, D. X., Chang, L., Li, J. H., and Yin, Z. J. (2021). Migration and accumulation of crude oils in the Qionghai Uplift, Pearl River Mouth Basin, Offshore South China Sea. *J. Pet. Sci. Eng.* 205, 108943. doi: 10.1016/j.petrol.2021.108943

Xie, H., Zhou, D., Li, Y., Pang, X., Li, P., Chen, G., et al. (2014). Cenozoic tectonic subsidence in deepwater sags in the Pearl River Mouth Basin, Northern South China Sea. *Tectonophysics* 615–616, 182-198. doi: 10.1016/j.tecto.2014.01.010

Yang, X. Y., Zhu, J. Z., Zhu, M., Long, Z. L., Xiong, W. L., Zheng, Y. D., et al. (2022). Geochemical characteristics of light hydrocarbons in condensate oil from the Southwestern Huizhou of the Pearl River Mouth Basin. *Bull. Geol. Sci. Technol.* 41 (4), 100–108. doi: 10.19509/j.cnki.dzkq.2022.0116

Zecchin, M., and Catuneanu, O. (2015). High-resolution sequence stratigraphy of clastic shelves III: Applications to reservoir geology. *Mar. Petrol. Geol.* 62, 161–175. doi: 10.1016/j.marpetgeo.2014.08.025

Zeng, Z. W., Zhu, H. T., Yang, X. H., Zeng, H. L., Xia, C. C., and Chen, Y. (2019). Using seismic geomorphology and detrital zircon geochronology to constrain provenance evolution and its response of Paleogene Enping Formation in the Baiyun Sag, Pearl River Mouth Basin, South China Sea: Implications for paleo-Pearl River drainage evolution. *J. Pet. Sci. Eng.* 177, 663–680. doi: 10.1016/j.petrol.2019.02.051

Zhang, X. (2019). Sequence stratigraphy and evolution of the deltaic depositional systems of early-middle Miocene shelf prim in the northern Pearl River Mouth Basin (Beijing: China University of Geosciences), 1–143.

Zhang, X. H., Zhang, C. M., Hartley, A., Xu, Q. H., Feng, W. J., Yin, T. J., et al. (2023). Analysis of the sedimentary characteristics of a modern distributive fluvial system: A case study of the Great Halten River in the Sugan Lake Basin, Qinghai, China. *J. Earth Sci.* 34 (4), 1249–1262. doi: 10.1007/s12583-022-1715-0

Zhao, Q. G., Jian, Z. M., Wang, J. L., Cheng, R. X., Huang, B. Q., Xu, J., et al. (2001). Neogene oxygen isotopic stratigraphy, ODP Site 1148, northern South China Sea. *Sci. China Ser. D: Earth Sci.* 44, 932–942. doi: 10.1007/BF02907086

Zhou, L. Y., Liu, J., Saito, Y., Liu, J. P. L., Li, G. X., Liu, Q. S., et al. (2014). Fluvial system development and subsequent marine transgression in Yellow River (Huanghe) delta and its adjacent sea regions during last glacial maximum to early Holocene. *Cont. Shelf Res.* 90, 117–132. doi: 10.1016/j.csr.2014.06.012

Zhou, W., Wang, Y. M., Gao, X. Z., Zhu, W. L., Xu, Q., Xu, S., et al. (2015). Architecture, evolution history and controlling factors of the Baiyun submarine canyon system from the middle miocene to quaternary in the Pearl River Mouth Basin, northern south China sea. *Mar. Petrol. Geol.* 67, 389–407. doi: 10.1016/j.marpetgeo.2015.05.015

Zhu, M., Graham, S., Pang, X., and Mchargue, T. (2010). Characteristics of migrating submarine canyons from the middle miocene to present: implications for paleoceanographic circulation, northern south China Sea. *Mar. Petrol. Geol.* 27, 307–319. doi: 10.1016/j.epsl.2015.03.032